Investigations into enhanced wax production with combustion synthesized Fischer Tropsch catalyst

Article *in* Energy Conversion and Management · February 2016

Impact Factor: 4.38 · DOI: 10.1016/j.enconman.2016.02.075

2 authors:

Snehesh Shivananda

Indian Institute of Science

7 PUBLICATIONS **3** CITATIONS

SEE PROFILE

Dasappa S.

Indian Institute of Science

114 PUBLICATIONS **920** CITATIONS

SEE PROFILE

Energy Conversion and Management 116 (2016) 80–90

Contents lists available at ScienceDirect

Energy Conversion and Management

journal homepage: www.elsevier.com/locate/enconman

Investigations into enhanced wax production with combustion synthesized Fischer–Tropsch catalysts

Snehesh Shivananda Ail, S. Dasappa *

Center for Sustainable Technologies, Indian Institute of Science, Bangalore 560012, India

ARTICLE INFO

Article history:
Received 25 November 2015
Accepted 26 February 2016

Keywords:
Fischer–Tropsch
Higher hydrocarbons
Liquid fuel
Combustion synthesis catalysts
Silica doped alumina
Metal support interaction

ABSTRACT

Combustion synthesized (CS) cobalt catalysts deposited over two supports, alumina and silica doped alumina (SDA), were characterized and tested for its Fischer–Tropsch (FT) activity. The properties of CS catalysts were compared to catalysts synthesized by conventional impregnation method (IWI). The CS catalysts resulted in 40–70% increase in the yield of C_{6+} hydrocarbons compared to IWI catalysts. The FT activity for CS catalysts showed formation of long chain hydrocarbon waxes (C_{24+}) compared to the formation of middle distillates (C_{10}–C_{20}) for IWI synthesized catalysts, indicating higher hydrocarbon chain growth probability for CS catalysts. This is ascribed to the smaller crystallite sizes, increased degree of cobalt reduction and consequentially, a higher number of active metal sites exposed over the catalyst surface. Additionally, 12–13% increase in the overall C_{6+} hydrocarbon yield is realized for SDA-CS catalysts, compared to Al_2O_3-CS catalysts. The improved performance of CS-SDA catalysts is attributed to 48% increase in cobalt dispersion compared to Al_2O_3 supported CS catalysts, which is again caused by the decrease in the cobalt-support interaction for SDA supports. The metal support interactions were analyzed using XPS and H_2 TPR–TPD experiments. Combustion method produced catalysts with smaller crystallite size (17–18 nm), higher degree of reduction (~92%) and higher metal dispersion (16.1%) compared to the IWI method. Despite its enhanced properties, the CS catalysts require prominently higher reduction temperatures (~1100–1200 K). The hydrocarbon product analysis for Al_2O_3 supported catalyst showed higher paraffin wax concentrations compared to SDA supported catalysts, due to the lower surface basicity of Al_2O_3. This work reveals the impact of the CS catalysts and the nature of support on FT activity and hydrocarbon product spectrum.

1. Introduction

Escalating energy demands due to depleting petroleum sources has renewed interests in Fischer–Tropsch (FT) process. FT synthesis reaction is at the core of gas to liquid (GTL) process and can be used to convert natural gas, coal or biomass to liquid transportation fuel [1]. Recently, biomass to liquid (BTL) process has attracted much attention for producing environment friendly, carbon neutral diesel from biomass [2]. In this process, biomass is subjected to gasification to generate syngas (mixture of CO and H_2), followed by conversion to higher hydrocarbons via the FT process [3,4]. The hydrocarbon products are cracked to produce high quality diesel that are characterized by high cetane number and are generally devoid of sulfur, nitrogen or aromatic compounds [5]. High quality diesel is obtained in large quantities (nearly 80 wt.% of the total products) using cobalt catalysts in the low temperature FT (LTFT) reaction. The LTFT reactors, operating in the temperature range of 463–513 K, predominantly yield waxes as a major products. The commercially operating FT reactors maximize the production of diesel by mild hydrocracking of waxes. The major advantage of this particular process is that the wax can be hydrocracked completely to diesel, yielding nearly 80% diesel fractions. Moreover, the diesel obtained by hydrocracking of waxes has higher degree of branching that gives it an advantageous lower pour point and also has nearly zero aromatic content, rendering it a high quality fuel [6]. Leckel [7] described a process scheme that maximizes this high quality diesel yield from an LTFT reactor, wherein nearly two-thirds of the final diesel is obtained from the wax hydrocracker while the remaining one-third is obtained from the fractionation of the hydrotreated LTFT condensation fraction. Overall, the FT products range from low molecular weight hydrocarbons to long chain waxes. The products obtained are a direct function of reaction conditions (temperature, pressure, space velocity) and catalytic properties.

* Corresponding author. Tel.: +91 80 23600536; fax: +91 80 23601692.
E-mail addresses: snehesh@cgpl.iisc.ernet.in, snehesh.s@gmail.com (S.S. Ail), dasappa@cgpl.iisc.ernet.in (S. Dasappa).

http://dx.doi.org/10.1016/j.enconman.2016.02.075
0196-8904/

Catalyst synthesis procedure and choice of supports have a broad effect on FT activity and selectivity. Several supports like Al_2O_3, SiO_2, TiO_2, alumino-silicates and carbon nanofibers have been investigated for its effect on FT activity [8–11]. Though the fundamental operation of a support is just of physical nature, i.e. to increase the amount of surface area available for reactants, very often the dispersed metals show a strong affinity for the support, eventually altering the catalytic activity [12]. FT active metals, cobalt and iron, deposited over oxide supports show a distinct metal-support interaction and depending on the nature of this interaction FT activity is dynamically affected. Detailed work on the influence of choice of support on FT reaction has been given by Storsæter et al. [13]. The extent of metal reduction was shown to be the least for Al_2O_3 supported catalysts, and highest for SiO_2 supported catalysts, indicating a stronger metal support interaction for Al_2O_3 compared to SiO_2 supported catalysts. For cobalt–alumina system, the formation of cobalt aluminate species over Al_2O_3 supports further reduce the available active sites for FT synthesis [13]. Apart from the formation of bulk aluminates over Al_2O_3 supports, the degree of reduction and hence the metal dispersion reduces due to the formation of $Co_{2+}Co^{3+}_{2-x}Al_xO_4$ mixed spinels, additionally reducing the FT activity [14,15].

More recently, several researchers have investigated the properties of FT active metals supported over silica doped alumina (SDA). Catalysts characterized by Jean-Marie et al. [16], showed lower concentrations of cobalt aluminate compounds in SDA compared to alumina supported catalysts. The use of SDA support with composition of 5% SiO_2 and 95% Al_2O_3, significantly enhanced the cobalt reducibility, resulting in 18% increase in CO conversion [16]. The work by Daniell et al. [17] reported formation of Lewis and Bronsted acid sites by addition of SiO_2 to γ-Al_2O_3. Moreover, the quantity and the strength of these acid sites were highest for 40% SiO_2 weight fraction in the synthesized supports [17]. Consequently, the amount of acid sites has a direct influence on the FT product spectrum. Low acidity catalysts produce hydrocarbon products comprising mostly straight chain alkenes and alkanes. More acidic catalysts result in FT products comprising lighter and more branched hydrocarbons [18].

The catalyst synthesis conditions display pronounced effect on the FT activity, hydrocarbon selectivity and product distribution. Catalyst synthesis involves introduction of metal precursor into supports of high surface area and calcination of the deposited metal salt into its oxide form. For the FT reaction, the metal oxide is further reduced to its zero valent form by H_2 reduction step. Addition of metal salts into the catalyst carrier is achieved most commonly by incipient wetness impregnation (IWI) method and co-precipitation method. The combustion synthesis (CS) method of catalyst preparation has been used for synthesis of large number of metal oxides [19–29] and can be applied for synthesizing supported cobalt catalysts for FT reactions. The CS method, also referred to as self-propagating high temperature synthesis, is an efficient approach for developing metal oxides, wherein the heat required for the decomposition of the metal precursors to its corresponding metal oxides is generated by the exothermic redox reaction of a fuel and an oxidizer. The synthesis process includes impregnation of a mixture of fuel (urea, citric acid, hydrazine, etc.) and oxidizer (active-metal salts like cobalt nitrate) into the support extrudes and ignition of this mixture by an external heating source. The combustion of this mixture generates a high temperature reaction wave across the volume causing decomposition of the mixture precursors and resulting in the formation of metal oxides. The major limitation for CS process is the high heat release and the consequential high temperature rise rates (~200–300 K/min), resulting in the evolution of combustion products with uncontrolled explosion, eventually powdering the catalysts and in most cases resulting in the loss of active components. Such vigorous behavior of CS reaction is distinctly evident for metal loading >8–10% [22]. The use of these powdered catalysts in a fixed bed reactor demands either re-pelletizing or re-molding which is considered very disadvantageous [30].

Shi et al. [31] synthesized SiO_2 supported Co catalysts by combustion synthesis and reported a CO conversion of 46.5% compared to 16.7% for IWI synthesized catalysts. The increased CO conversion was primarily attributed to reduced crystallite size, increased degree of reduction and higher metal dispersion for CS catalysts. In another work, FT active SiO_2 catalysts were synthesized by Shi et al. [32] in a single step without the need for further reduction. This was achieved by maintaining an equivalence ratio (the ratio of the actual fuel-to-oxidizer ratio to the stoichiometric fuel-to-oxidizer ratio) of 1.5 and a non-oxidizing environment during the combustion step. Though a remarkable method of synthesizing active catalyst, the authors in their work have not reported the crucial information indicating the effect on hydrocarbon product selectivity or product distribution. LeViness et al. [33], in their work reported the use of silica cobalt catalysts synthesized by the proprietary *organic matrix combustion process*, used in a microchannel reactor. The authors reported an average CO conversion of 70%, CH_4 selectivity of 7%, and a C_{5+} selectivity of 88%. The productive reaction performance was achieved by improved catalyst properties and efficient reactor performance.

In the present study, the combustion synthesis of 20 wt.% cobalt on alumina and, silica doped alumina support extrudes has been explored. The synthesized catalysts are characterized to understand the impact on metal support interaction as a consequence of the synthesis mechanism and its influence on the FT activity and product selectivity. Catalysts are characterized using DTA–TGA, FTIR, TPR–TPD, XRD, and XPS. The investigations conducted confirm the influence of support and the role combustion synthesis method on the hydrocarbon chain length formed. Properties of CS catalysts and its FT activity are compared with the catalysts synthesized by IWI method.

2. Experimental procedure

2.1. Catalyst synthesis

The redox mixture comprised of cobalt nitrate hexahydrate ($Co(NO_3)_2{\cdot}6H_2O$, Merck emplura) and hexamethylenetetramine ($C_6H_{12}N_4$, Alfa Aesar) as metal and fuel precursors respectively. The supports, γ-alumina and silica doped alumina (40 wt.% SiO_2/60 wt.% Al_2O_3) comprised of 1 mm spheres with a surface area of 158 m^2/g and 380 m^2/g respectively. The aqueous solution of metal and fuel precursors was impregnated in the supports by stirring in a rotary vacuum evaporator. Cobalt loading for CS catalysts was attained in multiple steps. IWI catalysts were synthesized by calcining the impregnated support in a furnace maintained at 823 K for a duration of 6 h.

The stoichiometry for the redox reaction was selected with the equivalence ratio of one, to achieve maximum heat release. As described by Eq. (1), the metal nitrate to fuel molar ratio is 3.86. The impregnated catalyst spheres were calcined in a muffle furnace, and the temperature increased to 673 K at 10 K/min. To measure the combustion reaction temperature, a known mass of the redox-mixture impregnated support is placed in a beaker and heated in a muffle furnace. An R-type (1 mm diameter) thermocouple is inserted into this beaker which contains the impregnated support. The reaction temperature is recorded using a P-Daq data acquisition system. Further, the redox mixture is heated by increasing the furnace temperature at the rate of 10 K/min using a PID controller. Once the reaction gets initiated, a reaction wave

spans throughout the support volume forming cobalt oxide. The theoretical estimation of the maximum temperature achieved during the combustion reaction was estimated by the method described in Turns [34].

$$27Co(NO_3)_2 \cdot 6H_2O + 7C_6H_{12}N_4 \rightarrow 9Co_3O_4 + 41N_2 + 204H_2O + 42CO_2 \quad (1)$$

2.2. Catalyst characterization

The FT-IR spectra of impregnated supports and calcined catalysts are examined to investigate the nature of the redox complex and to probe if any combustion residues are remaining on the support surface. The samples are scanned from 4000 cm^{-1} to 400 cm^{-1} with a resolution of 4 cm^{-1} using a Perkin Elmer 100 FT-IR spectrometer coupled with ATR accessory.

The combustion thermal events are characterized with Perkin Elmer STA-6000 analyzer to obtain the real-time measurements and analysis of sample weight change and heat flow. The sample is heated at the rate of 5 K/min in static air starting from initial temperature of 313 K to a maximum temperature until no weight loss is observed ($dm/dt = 0$), indicating completion of the combustion reaction.

X-ray diffraction spectra were recorded by a Rigaku Smartlab X-ray spectrometer to identify to cobalt oxide phases in the synthesized catalysts. The 2-θ values were scanned at a rate of 0.2°/min from 30° to 70° with Cu Kα radiation (λ = 1.54 Å). Scherrer formula was used to calculate the crystalline sizes of the synthesized catalysts from the line broadening. Instrumental line broadening is evaluated using the XRD spectra of Si-polycrystalline standard and peak broadening due to strain is neglected. Effective peak broadening is then incorporated into the Scherrer equation to obtain the crystallite size.

Temperature programmed reduction and desorption (TP**X**, X = reduction/desorption) studies are performed in a Micrometrics Autochem 2920 TPX system. The analysis of obtained TPD profiles gives the total number of active cobalt sites on the support surface, and also provide the nature of metal support interaction. The methods applied by Sewell et al. [35] for evaluation of degree of reduction (DoR(%)) and metal dispersion (D(%)) have been used as described in Eqs. (2) and (3).

$$\mathrm{DoR}(\%) = \frac{N_{H2-ads} * 58.93}{m_{cat} * L * SF} * 100 \quad (2)$$

$$D(\%) = \frac{N_{H2-des} * 2 * 58.93 * 10^4}{L * m_{cat} * \mathrm{DoR}} * 100 \quad (3)$$

Here, N_{H2-ads} is the H_2 uptake from the TPR spectra, L is the percentage metal loading, SF is the Co^0 reduction stoichiometric factor (1.33), m_{cat} is the mass of catalyst used for the TPR and TPD process. Approximately 50 mg of sample is weighed and placed in a U-shaped quartz cell. All TPX studies include conditioning of the sample by heating in Ar at 473 K for two hours, to remove any associated moisture traces. The quartz cell is cooled to 373 K and the gas line switched to 10% (vol%) H_2/Ar with a flow rate of 10 ml/min. The furnace temperature is increased to 1273 K at the rate of 10 K/min. H_2 consumption is measured using a TCD detector. The amount of chemisorbed H_2 is measured by reducing ~30 mg of catalyst in pure H_2 (purity >99.995%) for 16 h and then cooled to 373 K. At this temperature, the gas flow is switched to Ar, and the flow is maintained for one hour to remove physisorbed H_2. The catalyst cell is then ramped to 773 K at a rate of 20 K/min in Ar flow to desorb the chemisorbed H_2. The recorded TPD spectrum is analyzed to quantify the chemisorbed H_2. Total active sites and the cobalt dispersion are calculated assuming dissociative H_2 chemisorption with stoichiometry factor of 0.5.

NH_3-TPD data were obtained to determine the surface acidity and the total number of acid sites on the supports and synthesized catalysts. Around 30 mg of sample is placed in the quartz sample holder and saturated with NH_3 at 373 K for two hours. The gas flow is then switched to Ar with a flow rate of 50 ml/min at the same temperature for an hour to remove physisorbed NH_3. The sample temperature was then increased to 700 K at 20 K/min. The amount of desorbed NH_3 is recorded to determine the number of acidic sites.

XPS information is obtained on AXIS ULTRA system with Al Kα radiation ($h\nu$ = 1486.6 eV), operated at 15 kV, 10 mA and ambient temperature with the vacuum of 10^{-8} Torr. The narrow region of core level spectra of the calcined and reduced catalysts are analyzed to obtain information on the cobalt oxidation state. The XPS spectrum peak shift is corrected using the binding energy (B.E.) of C-1s spectra observed at 284.8 eV. The raw XPS data are deconvoluted using CasaXPS software to separate the contributions from various oxide phases.

2.3. Fischer–Tropsch activity studies

FT experiments are performed in a fixed bed reactor at 3 MPa and 503 K. Experimental layout involved in this work is shown in Fig. 1. The syngas feed consists of 70% H_2 and 30% CO volumetric gas composition. The inlet gas flow rate of is controlled by Brooks mass flow controller and the pressure in the reactor is regulated using TESCOM ER-5000 BPR. Catalyst bed temperature is measured using an axially inserted resistance temperature detector (RTD) and the reactor temperature is controlled using a proportional–integral–derivative (PID) controller. The synthesized catalysts, prior to FT reactions, are reduced in H_2 (purity = 99.995%), at a temperature of 1200 K, for a duration of 20 h. Six grams of reduced catalysts are mixed with 25 g of βSiC, to maintain isothermal bed conditions, and transferred carefully into the FT reactor. Gas composition and exit gas flow rates are recorded for a duration of 85 h, after a stabilization period of 24 h. Exit gas composition is measured using an online Perkin Elmer Clarus 680 gas chromatograph with an *elite*-Alumina column. The product transfer line connecting the exit of the FT reactor to the condenser is maintained at 423 K to prevent the condensation of any hydrocarbon products. The higher hydrocarbons are separated in a gas–liquid separator consisting of a cold trap maintained at 273 K and a hot trap maintained at 373 K. Liquid samples are analyzed, after every run in a Perkin Elmer Clarus SQ8C-MS. Eqs. (4) and (5) evaluate the percentage CO conversion (χ_{CO}(%)) and percentage hydrocarbon selectivity (S_{CH*}(%)). Here, m^*_{CO-in}, m^*_{CO-out} are the mass flow rates of CO entering and leaving the system and m^*_{CH*} is the mass flow rate of the hydrocarbon product specie.

$$\chi_{CO}(\%) = \frac{m^*_{CO-in} - m^*_{CO-out}}{m^*_{CO-in}} * 100 \quad (4)$$

$$S_{CH*}(\%) = \frac{m^*_{CH*}}{m^*_{CO-in} - m^*_{CO-out}} * 100 \quad (5)$$

3. Results and discussions

This section details the catalyst characterization results, indicating the redox combustion properties for the selected CS stoichiometry, the reduction behavior of cobalt oxides, the cobalt crystallite size and the nature of metal support interaction for

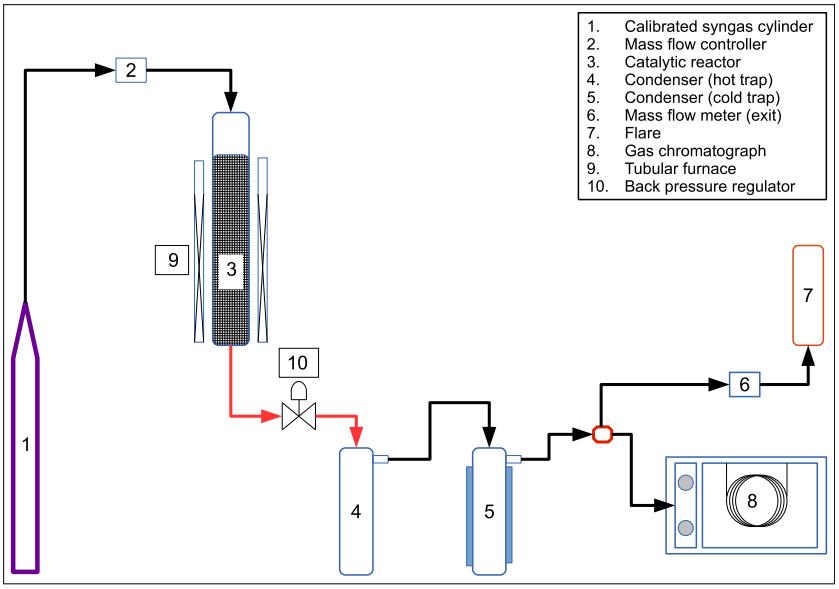

Fig. 1. Fischer–Tropsch activity test setup.

the synthesized catalysts. Further, the section describes the effect of the developed catalysts on the Fischer–Tropsch reaction.

3.1. Catalyst characterization

3.1.1. Combustion thermodynamics

CS catalysts are synthesized with a reaction stoichiometry such that the impregnated redox mixture react over the support surface without any residual traces of carbonaceous products or unburnt fuel and metal precursors, resulting only in the formation of cobalt oxide. Hence, the fuel-to-oxidizer ratio should be such that, sufficient energy is generated in a self-sustained state for the complete decomposition of fuel and metal precursor into cobalt oxide and gaseous products, viz., CO_2, N_2, and H_2O. Maximum theoretical temperature of 1457 K was obtained for the selected redox reaction using the thermodynamic data listed in the Supplementary Material link, identified as Table SM-A.

Fig. 2 shows the temperature–time profile for hexamethylenetetramine (HMTA) and cobalt nitrate redox reaction with an oxidizer to fuel molar ratio of 3.86. Two stages of combustion are observed. The first stage, observed from the reaction initiation at 421 K to 480 K with a slope of 15 K/min, is due to the commencement of surface combustion reaction. The second stage, as observed from 480 K to a maximum temperature of 571 K, is accounted for the redox reaction of bulk NO_3^- and the fuel with the temperature rise rate of 180–200 K/min.

CS reactions are marked by rapid heat release rates and large rates of product formation, resulting in an uncontrolled combustion process, especially for metal loading greater than 5% and eventually forming powdered catalysts. This factor has prevented extensive use of CS for catalyst synthesis, especially for reactions like Fischer–Tropsch, which require metal loading >15–20% [36,37,11,38]. In the current study, catalysts with metal loading of 20% have been achieved on spherical supports for direct use in a fixed bed reactor.

The thermal events that occur in the course of redox reaction were recorded using a DT–TGA analyzer. Fig. 3 shows the DT–TGA profile for CS and IWI impregnated catalysts. The redox reactions occur in the temperature range of 430–520 K, where a total weight loss of 25% is observed. Region I for CS catalysts, as seen from 430 K to 455 K, shows 4.5% sample weight loss. The exothermic reactions that occur in this region correspond to the surface combustion of NO_3^- and HMTA. In region II, observed from 455 K to 475 K, the sharp exothermic peak corresponds to the redox reac-

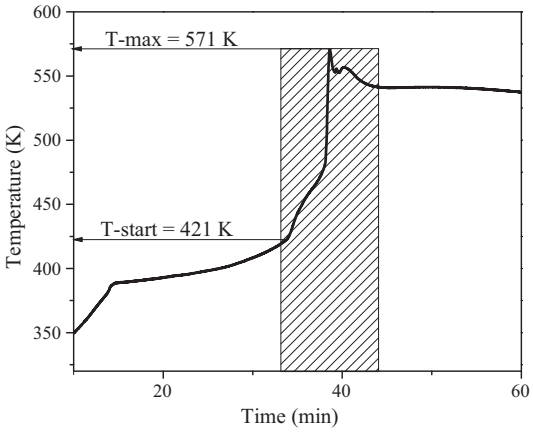

Fig. 2. Temperature time profile for HMTA-$Co(NO_3)_2{\cdot}6H_2O$ reaction.

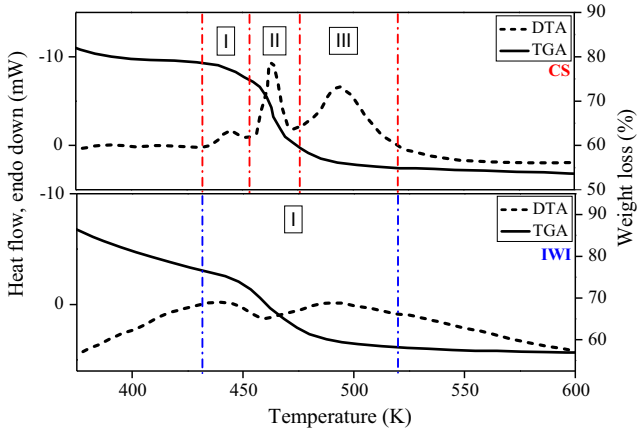

Fig. 3. Simultaneous thermogravimetric and differential thermal analysis for CS and IWI catalysts.

tion of bulk NO_3^- and HMTA. A maximum weight loss of 16% is observed in this region. The weight loss observed in region III is due to the redox reaction of residual fuel–oxidizer mixture, as observed from 476 K to 521 K, accounting for 5% sample weight loss. The thermal behavior observed for IWI catalysts shows a broad weight loss region with an endothermic decomposition of $Co(NO_3)_2{\cdot}6H_2O$, resulting in the formation Co_3O_4. The weight loss curve for CS catalysts shows clearly that the selected stoichiometry produces enough heat for decomposition of cobalt nitrate resulting in the formation of supported Co_3O_4.

Fourier transform infrared (FT-IR) spectroscopy of the fuel–oxidizer mixture and the burnt catalysts were examined to primarily investigate the nature of the redox complex and to probe the completion of the combustion reaction. Fig. 4 shows the FT-IR spectrum of the impregnated redox mixture and the calcined catalysts. The distinct peak observed at 1360 cm^1, which splits at 1313 cm^1 and 1296 cm^1, corresponds to the symmetric stretching of mono-dentate nitrate ion. The split band spectra indicate the coordination of HMTA to the Co ion. HMTA, a tetradentate ligand, complexes with metal ions and acts as a combustion precursor for the complex metal ions [24]. The broad peak observed at 3352 cm^1 indicates the presence of moisture in the sample and the peak identified at 819 cm^1 corresponds to the vibration spectra of CH_2 rocking. For calcined catalysts, the FT-IR spectra show no existence of the redox precursors or the combustion residues, further supporting complete combustion of the redox mixture.

3.1.2. Temperature programmed reduction and desorption

Fig. 5 shows the H_2 reduction profile for the synthesized catalysts. Primary observations, as seen from the plots, reveal that the synthesis procedure and the nature of support used, have a profound effect on the catalyst reduction temperatures as well as the degree of reduction. For IWI synthesized SDA supported catalysts, H_2 reduction peaks are observed at 547 K, 611 K and 909 K. The initial two peaks correspond to the twin-step reduction of Co_3O_4 ($Co_3O_4 \longrightarrow CoO \longrightarrow Co$), whereas the broad peak observed at the higher temperature are due to reduction of various phases of cobalt oxides formed on the support surface. The reduction of various phases of cobalt oxides supported on Al_2O_3 was investigated by Arnoldy and Moulijn [39], where four stages of cobalt oxide were reported, corresponding to the four different types of cobalt phases on Al_2O_3. Phase-1 (T_1 = 550–580 K) corresponds to the twin step reduction of Co_3O_4, as described earlier. Phase-2, as described by Arnoldy and Moulijn [39], represents Co^{3+} ions in Co_3-AlO_6 crystallites, with reduction peak at 750 K. For CS catalysts, minimal H_2 uptake is observed, though some traces of H_2 consumption are observed for IWI catalysts. Phase-3 consists of the reduction of surface Co^{2+} ions, as observed at 900 K. A strong peak for Al_2O_3-CS is observed at 915 K (T_3), clearly indicating the reduction of surface Co^{2+} ions. Phase-4 as expressed by Arnoldy and Moulijn [39], at temperature ~1200 K, includes the reduction of surface or subsurface Co^{2+} ions in the Co^{2+}–Al^{3+} spinel structure. From the TPR profile observed in Fig. 5, it is evident that the spinel structures continue to get reduced at temperatures above 1000 K. H_2 consumption is not observed for IWI catalysts above 1000 K. The irreducible cobalt oxide species that reduce at temperatures above 1200 K have been reported by Schanke et al. [40], Jabłoński et al. [41], Arnoldy and Moulijn [39]. It is likely that these species are present in IWI synthesized catalysts which occur in a stable form at low temperatures [42].

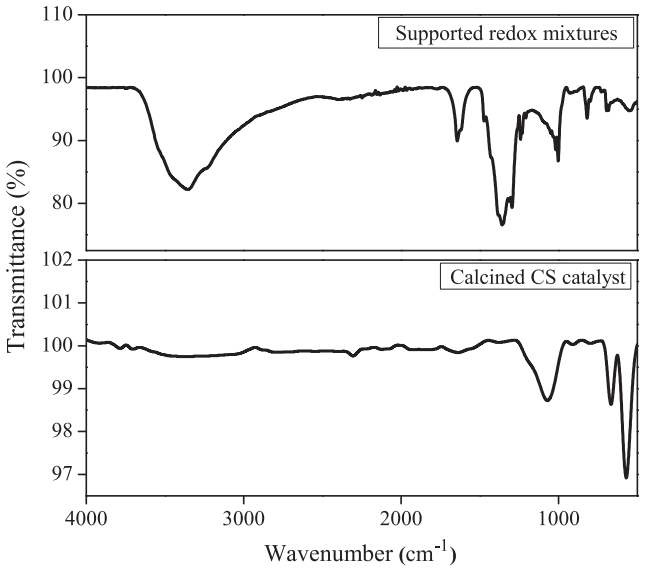

Fig. 4. FT-IR of supported redox precursors and calcined catalysts.

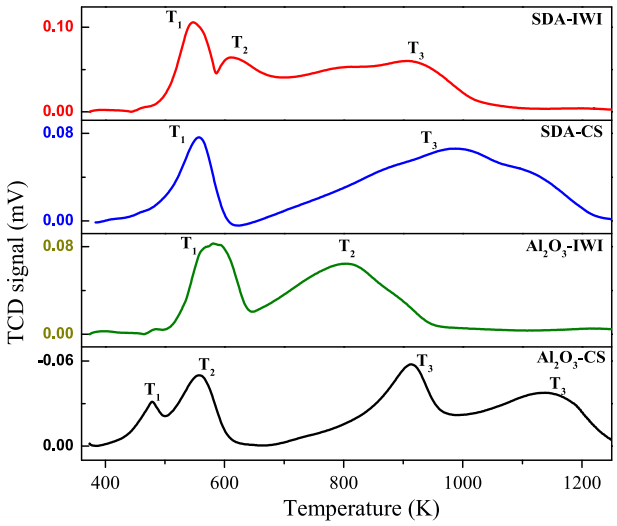

Fig. 5. Temperature programmed reduction of IWI and CS catalysts.

The reduction temperatures of the synthesized catalysts, the degree of reduction and the cobalt dispersion are tabulated in Table 1. As seen from the table, the degree of reduction for IWI synthesized, silica doped alumina catalysts is higher than Al_2O_3 supported catalysts by 27%. The higher degree of reduction for SDA supported cobalt catalysts is due to the reduced formation of cobalt aluminates. Alteration of the Al_2O_3 support surface by the addition of SiO_2 results in the formation of alumino-silicates that impede the formation of barely reducible cobalt aluminates. It is evident from Table 1 that the total fraction of active Co^0 sites increases to 12.1% for IWI-SDA supported catalysts from 8.1% for IWI-Al_2O_3 supported catalysts, indicating a 41% increase in the metal dispersion. In case of SDA supported catalysts, the dispersion

Table 1
TPR–TPD summary.

Catalyst	Reduction temperatures			DOR (%)[a]	D (%)[b]
	T_1 (K)	T_2 (K)	T_3 (K)		
SDA-IWI	547	611	909	81	12.1
SDA-CS	557	–	986	92	16.1
Al_2O_3-IWI	581	801	–	63.85	8.6
Al_2O_3-CS	479	558	913; 1140	68.72	10.9
Co_3O_4	512	574	–	–	–

[a] From TPR H_2 uptake.
[b] From H_2 TPD of reduced catalysts.

increases from 12.1% for IWI catalysts to 16.1% for CS catalysts and, for Al_2O_3 supported catalysts, the dispersion increases from 8.6% for IWI catalysts to 10.9% for CS catalysts. These results evidence higher fraction of active Co^0 over combustion synthesized catalysts. Combustion synthesized Co/SiO_2 catalysts reported by Shi et al. [32], showed increased reduction temperatures with the degree of reduction of 89% and an improved metal dispersion of 16.6% compared to a degree of reduction of 82% and metal dispersion of 3.1% for IWI synthesized catalysts.

Table 2 gives the magnitude of acid sites expressed as mmol NH_3/g_{cat}. As seen in the table, the SDA supported catalysts exhibit higher surface acidity compared to the Al_2O_3 supported catalysts. Daniell et al. [17], in their work, show the formation of highly acidic Lewis and Bronsted acid sites for silica doped alumina supports, with properties similar to those found in zeolites. Increased surface acidity is evident from higher NH_3 desorption from the catalyst surface.

3.1.3. X-ray diffraction

XRD pattern for the calcined catalysts showed distinct peaks corresponding to Co_3O_4. Figs. 6 and 7 show the XRD spectra for the calcined and reduced catalysts. The 2-θ peaks observed at 31.2°, 36.94°, 44.86°, 55.82°, 59.24° and 65.16° are consistent with the spectra of Co_3O_4. In case of Al_2O_3 supported catalysts, an additional peaks at 66.9° and a broad peak at 45.8°, that nearly merges with the 44.86° peak, indicate the presence of γ-alumina (*ICSD-40029; ICSD-95302* [43,44]). Al_2O_3 supported cobalt catalysts usually result in the formation of cobalt aluminates. However, due to the close and overlapping signatures of $CoAl_2O_4$ and Co_3O_4, it is extremely difficult to differentiate between the two structures using XRD alone. While comparing with the Al_2O_3 supported catalysts, minimum signatures of γ-Al_2O_3 are still observed in the SDA supported catalysts. Daniell et al. [17] in their work reported a silica encapsulation of Al_2O_3 for silica doping in the range of 30–60%.

Table 2
Surface acidity measured by NH_3-TPD.

Sample	Acid strength (mmol/g_{cat})
SDA	0.711
Al_2O_3	0.371
SDA-IWI	1.080
SDA-CS	1.230
Al_2O_3-IWI	0.576
Al_2O_3-CS	0.727

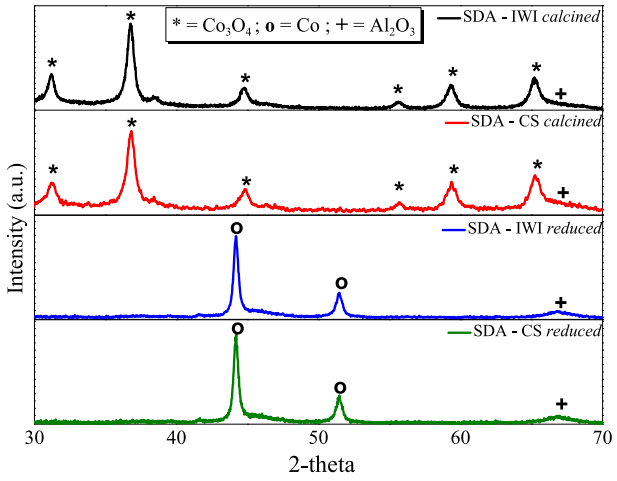

Fig. 6. XRD spectra of 20Co/SDA.

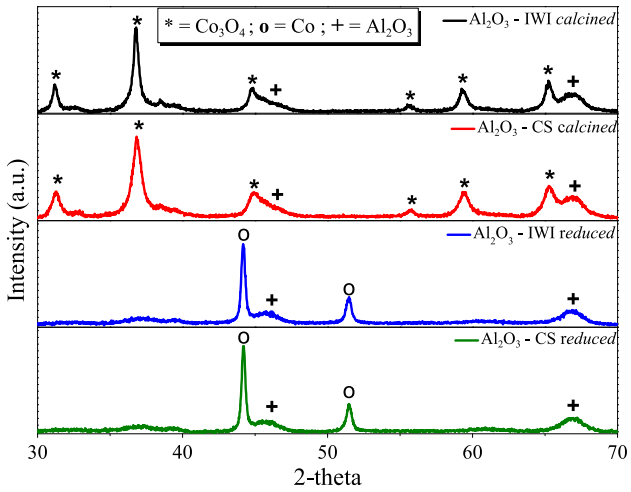

Fig. 7. XRD spectra of 20Co/Al_2O_3.

From the XRD results of the SDA supported cobalt catalysts, it is evident that minimum fractions of γ-Al_2O_3 phase still remain exposed on the catalyst surface. The XRD spectra of reduced catalysts show sharp 2-θ peaks at 44.2° and 51.5°, which correspond to metallic Co(*ICSD-53805* [45]). Furthermore, the Al_2O_3 supported reduced cobalt catalysts shows a low intensity peak at 67.24°, which corresponds to γ-Al_2O_3. The absence of this peak in SDA supported catalysts, further evidences the SiO_2 surface coverage. Table 3 shows the Co_3O_4 and Co^0 crystallite sizes for the synthesized catalysts. The cobalt crystallite size decreases by a margin of 30% for CS catalysts. The reduced crystallite size agrees with the dispersion estimate obtained from H_2 chemisorption experiments. A possible interpretation of the reduced crystallite size of CS catalysts can be obtained from the temperature–time experiments of the CS catalyst. As observed in Fig. 2, the CS catalysts are synthesized in a short span of 12–14 min. Contrarily, the IWI catalysts require a calcination time of 3–4 h for the complete decomposition of cobalt nitrate to cobalt oxide. The elongated calcination time for IWI catalysts is a probable cause for the sintering of cobalt crystallites resulting in catalysts with higher crystallite size compared to CS catalysts. Strikingly, the reduced catalysts were characterized by higher crystallite size, which is a likely outcome of the increased reduction temperature, since the crystallite size is expected to increase with temperature at constant pressure [46,47]. The crystallite size may increase by diffusion of mass from the outer layers of neighboring grains [46].

3.1.4. X-ray photoelectron spectroscopy

Figs. 8 and 9 show the deconvoluted spectra of the calcined catalysts. Decomposition of the XPS peaks enables the identification and quantification of the cobalt oxide phases present on the catalyst surface. Spectral mapping of the high resolution elemental spectra was obtained by *Gaussian curve fitting* routine, and the corresponding binding energy (B.E.) reference was obtained from the

Table 3
Crystallite sizes of the SDA and Al_2O_3 supported catalysts.

Catalyst	d_{Co3O4} (nm)[a]	d_{Co} (nm)[b]
SDA-IWI	14.1	26
SDA-CS	10.7	18.2
Al_2O_3-IWI	15.0	22
Al_2O_3-CS	10.5	17.6

[a] From XRD of calcined catalysts.
[b] From XRD of reduced catalysts.

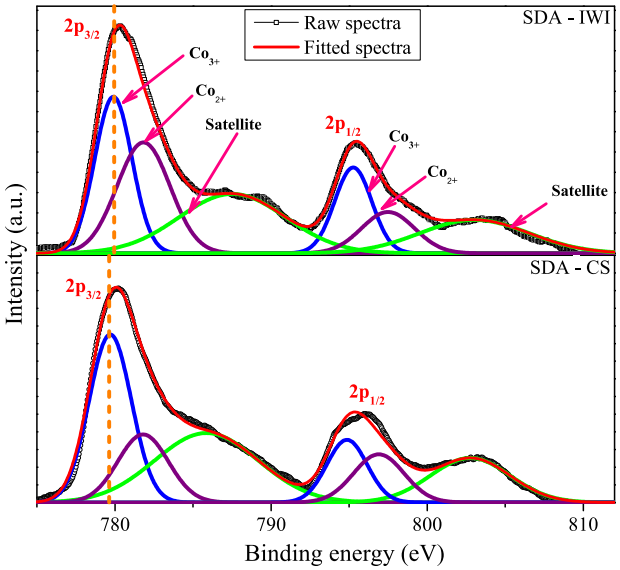

Fig. 8. XPS spectra of SDA supported cobalt catalysts.

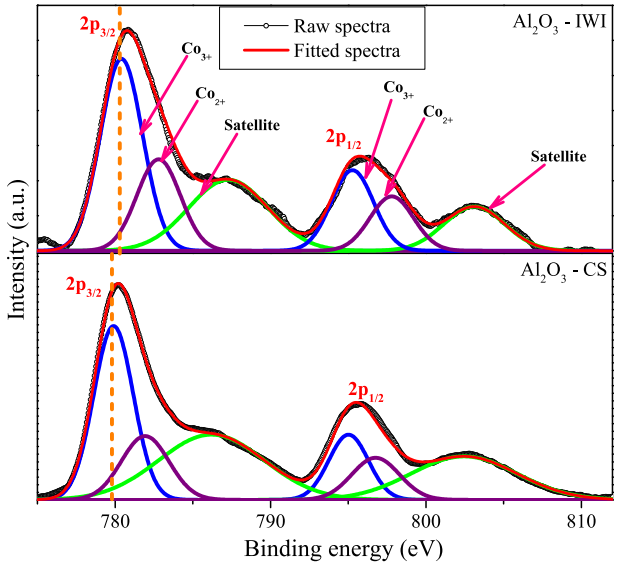

Fig. 9. XPS spectra of Al_2O_3 cobalt catalysts.

NIST database [48]. XPS spectra of Co_3O_4 standard was used to identify the binding energy (B.E.) of Co^{3+} and Co^{2+} oxidation states. The Co-$2p_{3/2}$ and the spin orbital splitting B.E. are listed in Table 4. The survey spectra of the Al_2O_3-IWI, Al_2O_3-CS, SDA-IWI and SDA-CS are shown in Supplementary material link, identified as Figure SM-I, SM-II, SM-III and SM-IV, respectively. The component at 779.9 eV for the deconvoluted spectra is referenced to Co_3O_4, which is the most dominant phase observed in the calcined catalysts. XRD of the calcined catalysts too revealed Co_3O_4 as the dominant phase. The second low intensity peak of the deconvoluted spectra corresponds to CoO. The satellite peaks observed at 783 eV, are indicative of CoO, and occur due to the charge transfer band structure, assigned to the late 3d transition metal oxides [49]. The information on the nature of the metal support interaction can be substantially obtained from the intensities of its satellite peaks. A higher concentration of the cobalt aluminates is indicated by the higher intensity of the shake-up satellites. This is because, $CoAl_2O_4$ has characteristics of strong shake-up satellites and has binding energies 6–7 eV higher than the main peak. Ji et al. [50] and Zsoldos et al. [51] reported stronger satellite intensity of CoO and $CoAl_2O_4$ specifying a stronger metal support interaction. The ratio of the intensities of Co-$2p_{3/2}$ peak at 779.9 eV to the intensity of the shake-up satellite peak points out the relative formation of $CoAl_2O_4$ in the synthesized catalysts. From Table 4, it is evident that the silica doping in Al_2O_3 drastically reduces the cobalt aluminate formation. Moreover, CS catalysts too revealed reduced aluminate formation, implying a lower metal support interaction compared to IWI catalysts.

Table 4
XPS summary.

Catalyst	B.E. Co-$2p_{3/2}$ (eV)	Spin-orbital splitting (eV)	I-Co$2p_{3/2}$/ I-shake-up	I_{Co}/I_{Al}
SDA-IWI	779.9	15.3	0.9	0.6
SDA-CS	779.7	15.2	1.1	1.6
Al_2O_3-IWI	780.4	15.2	0.7	0.2
Al_2O_3-CS	779.9	15.2	0.9	1.1
Co_3O_4-std	779.9	15.0	1.8	–

The measure of the cobalt dispersion can be obtained from the Al and Co peak intensity ratios [52,53]. Increasing intensity ratios indicate higher cobalt dispersion, revealing lower metal agglomeration. The percentage metal dispersion obtained from H_2 TPR–TPD experiments agree with the values obtained from XPS spectrum analysis. The metal dispersion as observed from the XPS spectral analysis shows that $D_{-Al2O3-IWI} \leqslant D_{-Al2O3-CS}$ and $D_{-SDA-IWI} \leqslant D_{-SDA-CS}$, further evidencing that the combustion synthesized catalysts result in higher degree of reduction, higher metal dispersion and consequently, larger number of active metal sites for the FT reaction. Additionally, the SDA supports display higher metal dispersion compared to alumina supported catalysts, signifying reduced metal support interaction for SDA supported catalyst.

3.2. FT activity and selectivity

The effect of the synthesized catalysts is shown in Fig. 10, where the activity and selectivity measurements were averaged over a duration of 85 h of operation. The synthesis procedure greatly enhances the FT activity and selectivity, resulting in higher CO conversion and C_{6+} selectivity for combustion synthesized catalysts, compared to conventionally impregnated catalysts. The CO conversion for SDA-CS catalysts increased to 42.9% from 33% as seen for SDA-IWI catalysts. A similar trend is observed for Al_2O_3 supported catalysts with 35% increase in CO conversion observed for CS catalysts. The C_{6+} selectivity increases by 4.5% for SDA-CS catalysts, but only a marginal increase of 0.7% is seen for Al_2O_3-CS catalysts. The FT activity of IWI and CS catalysts measured as the rate of CO consumption per unit mass of catalysts is shown in Fig. 11. The

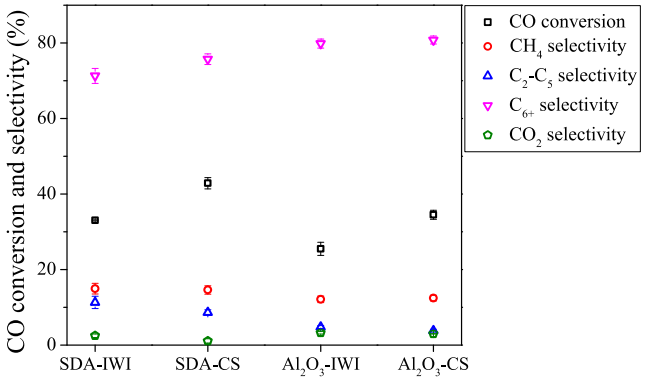

Fig. 10. CO conversion and selectivity for the synthesized catalysts.

increased performance of CS catalysts is attributed to its reduced cobalt crystallite size, increased degree of reduction and higher metal dispersion. A 2% decrease in the CH_4 selectivity is observed for SDA-CS catalyst compared to SDA-IWI catalyst while a 2.5% increase in CH_4 selectivity is observed for Al_2O_3-CS catalysts compared to Al_2O_3-IWI catalyst. The CO_2 selectivity varied from 1.1% for SDA-CS catalysts to a maximum of 3.3% for Al_2O_3-IWI catalysts. As seen in Fig. 10, the SDA supported cobalt catalyst displays higher selectivity for C_2–C_5 hydrocarbon fraction as compared to the Al_2O_3 supported cobalt catalyst. The C_2–C_5 selectivity for SDA-IWI and SDA-CS catalyst is 2.4 times higher than Al_2O_3-IWI and Al_2O_3-CS catalyst. The higher selectivity of C_2–C_5 hydrocarbons could be due to the existence of alumino-silicate structure occurring in the supports, giving it a zeolite-like behavior. A similar observation was reported by Fraenkel and Gates [54]. The higher C_2–C_5 selectivity for SDA supported catalysts results in lower C_{6+} selectivity, compared to Al_2O_3 supported catalysts.

The most striking feature observed is the FT product spectrum for the synthesized catalysts. The HC product distribution is observed to be a function of not only the synthesis procedure but also a function of the support material used. Figs. 12 and 13 show the weight fraction distribution of the liquid hydrocarbon products (C_{10}–C_{24}) and waxes (C_{24+}). The magnitude of active sites deposited over the supported catalysts and the degree of reduction are crucial factors that dictate the catalyst response for FT reaction. For SDA supported catalysts, the C_{24+} weight fraction increases from 0.01 wt.% for combustion synthesized catalysts to 0.6 wt.% for IWI catalysts. For Al_2O_3 supported catalysts, the C_{24+} weight fraction increases from 0.67 wt.% to 0.8 wt.%. The hydrocarbon chain growth probability factor, α, as described by the Anderson–Schulz–Flory (ASF) distribution model was determined for the synthesized catalysts based on the weight fraction of the various hydrocarbon species. The α value was evaluated from the ASF plot in the C_{10}–C_{24} hydrocarbon range (Fig. 12), as described in [55]. α increases from 0.89 for SDA-IWI catalysts to 0.94 for SDA-CS catalysts. For Al_2O_3 supported catalysts, α increases from 0.92 for IWI synthesized catalysts to 0.96 for CS catalysts. These values support the increased higher-hydrocarbon chain growth on the CS catalysts. The α values are comparable with the catalysts used in the Shell middle distillate synthesis process (α = 0.92–0.93) and with the Sasol's fixed bed reactor (α = 0.95) [56,57]. The experimental results clearly indicate that the hydrocarbon chain growth probability increases for catalysts synthesized by solution combustion

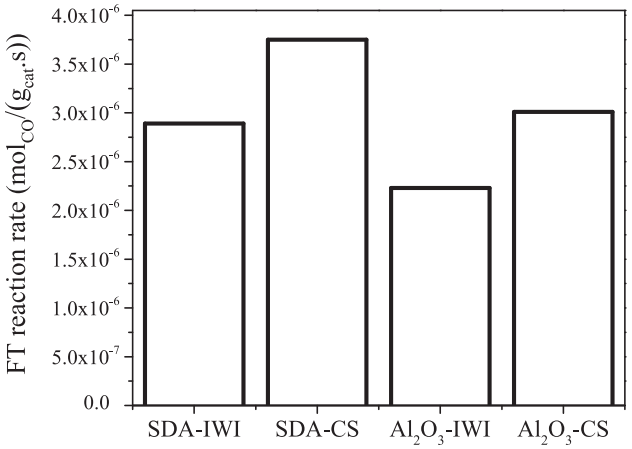

Fig. 11. FT activity of IWI and CS catalysts; P = 3 MPa, T = 503 K, WHSV = 2610 ml/(h·g$_{cat}$).

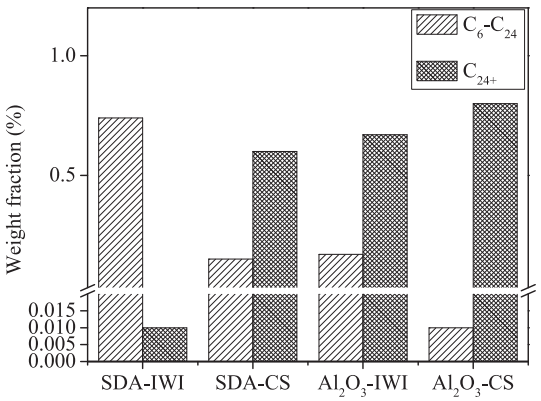

Fig. 13. Weight fraction of C_6–C_{24+} hydrocarbons in the FT products for the synthesized catalysts.

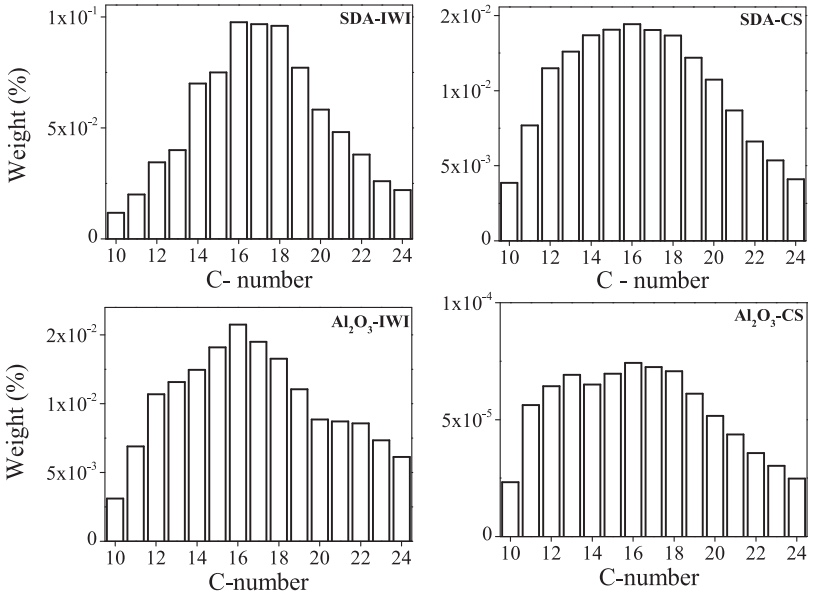

Fig. 12. Weight fraction of C_{10}–C_{24} hydrocarbon product distribution for the synthesized catalysts.

method, primarily due to the increased metal dispersion and higher catalyst reducibility.

Distinctly, the hydrocarbons synthesized over Al_2O_3 supported cobalt catalysts resulted in the formation of heavier waxes than middle distillates as compared to catalysts synthesized over SDA supports. The HC product spectrum for Al_2O_3-CS catalysts show 0.8 wt.% C_{24+} compared to 0.6 wt.% C_{24+} for SDA-CS catalysts. The 33% higher weight fraction of C_{24+} hydrocarbons for Al_2O_3 supported cobalt catalysts is due to the total number of acidic sites present in the SDA supports. The addition of silica to alumina results in the formation of stronger Bronsted acid sites, through bridged hydroxyl group formation across aluminum and silicon atoms [17]. Lower surface acidity results in FT product spectrum consisting primarily of lighter and more branched hydrocarbons [18,58–60]. NH_3-TPD of SDA supports, as seen in Table 2, show surface acidity of 0.7 mmol NH_3/g_{cat} compared to 0.4 mmol NH_3/g_{cat} for alumina supports, further supporting the acidic influence on the FT product spectrum.

The stability of the synthesized catalysts is evaluated by observing the activity and selectivity changes during the experimental run for a duration of 85 h. Fig. 14 shows the variation in CO conversion and hydrocarbon selectivity as a function of time on stream. In case of SDA supported catalysts synthesized by IWI and CS, the CO conversion, and HC selectivity remain steady for a duration of 85 h, indicating no possible catalyst deactivation. In case of Al_2O_3 supported catalysts synthesized by IWI method, the CO conversion drops from 31.4% to 19.6% indicating a 38% reduction in FT activity over a duration of 85 h, while a 10% reduction in the FT activity is recorded for Al_2O_3-CS catalysts. The observed spectrum in Fig. 14

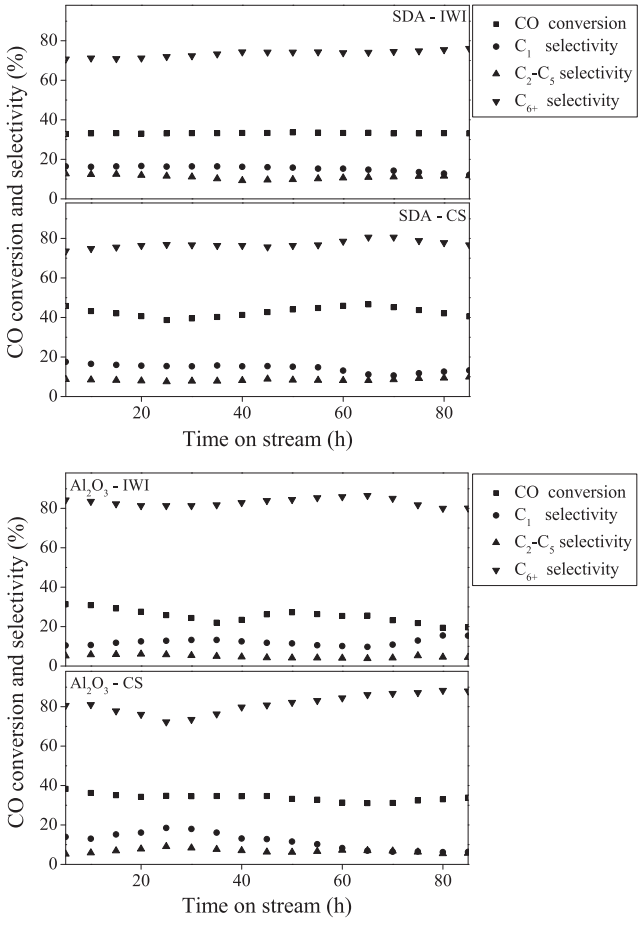

Fig. 14. CO conversion and selectivity variation with time on stream for the synthesized catalysts; *WHSV* = 2610 ml/(h·g_{cat}), *T* = 503 K, *P* = 3 MPa.

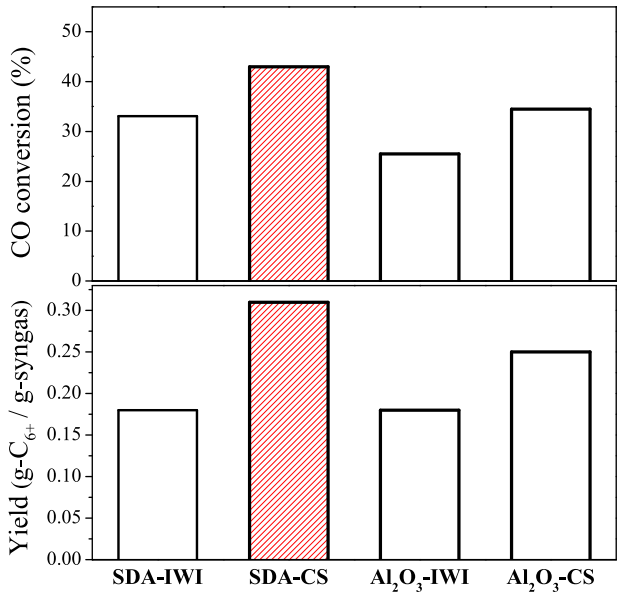

Fig. 15. C_{6+} yield comparison for the synthesized catalysts. *WHSV* = 2610 ml/(h·g_{cat}), *P* = 3 MPa, *T* = 503 K.

evidence that the combustion synthesized catalysts and silica doped alumina supports prevent catalyst deactivation as seen in Al_2O_3-IWI catalyst.

Fig. 15 compares the FT activity and product yield for the catalysts synthesized in this work. The SDA supported combustion synthesized catalysts show highest C_{6+} yield corresponding to 0.31 $g\text{-}_{C6+}/g\text{-}_{syngas}$, at a space velocity of 2610 ml/(h·g_{cat}). Overall, an improved FT performance is achieved with catalysts synthesized in this work. Fig. 15 clearly signifies an increase in the C_{6+} productivity for CS catalysts compared to IWI catalysts, with nearly 39% increase for CS-Al_2O_3 catalysts and ~70% increase for CS-SDA catalysts. While SDA-IWI catalysts produce a maximum concentration of liquid fuel fractions (C_{10}–C_{24}) compared to the other synthesized catalysts, the highest yield of higher hydrocarbons, that include liquid fuel and wax, is achieved by SDA-CS catalysts. With mild hydrocracking of waxes the yield of high quality diesel fractions can be greatly enhanced using SDA-CS catalysts.

4. Conclusions

The combustion synthesised cobalt catalysts show enhanced catalytic properties compared to the conventionally synthesized IWI catalysts, with respect to its reduced crystallite size, higher degree of reduction and higher metal dispersion. The primary reason of high metal dispersion for CS catalysts is attributed to reduced degree of metal sintering during the synthesis step, which is a common occurrence for IWI catalysts. Strikingly, the CS catalysts exhibit reduced fractions of cobalt aluminate formation that otherwise hider the degree of reduction resulting in decreased fraction of active cobalt sites. Compared to CS catalysts, the IWI catalysts reveal higher concentrations of the irreducible cobalt aluminates that contribute to its reduced dispersion and hence reduced FT activity. Moreover, while the silica doping of the alumina support is known to impede the formation of cobalt aluminates, the combined use of combustion synthesis method and the silica doped alumina support resulted in the formation of cobalt catalysts with improved properties, facilitating higher FT activity and higher C_{6+} selectivity. The investigations of the FT product spectrum revealed higher fractions of waxes (C_{24+}) with Al_2O_3 supported cobalt catalysts while hydrocarbons ranging from C_{10}–

C_{20} formed as the primary product for SDA supported catalysts. The differences in the nature of product spectrum is associated with the variation in the acidic characteristic of the Al_2O_3 and SDA supports – alumina being more basic compared to SDA, favoured the formation of waxes while SDA supported catalysts promoted the formation of middle distillates. Also, the hydrocarbon selectivity over CS catalysts resulted in higher wax formation compared to IWI catalysts, implying higher chain growth probability over CS catalysts, than over IWI catalysts. The overall hydrocarbon yield, measured as g_{C6+}/g_{syngas}, increases by a margin of 40–70% with the use of CS catalysts.

Acknowledgements

The authors wish to acknowledge financial support of Ministry of New and Renewable Energy (MNRE), Government of India and also the instrumentation facilities provided by National Centre for Combustion Research and Development (NCCRD), Centre for Nano Science and Engineering (CeNSE) at IISc Bangalore and National Environmental Engineering Research Institute (NEERI), Nagpur. Further, the authors would like to express their gratitude to Sasol Germany GmbH for providing the support materials used in this work.

Appendix A. Supplementary material

Supplementary data associated with this article can be found, in the online version, at http://dx.doi.org/10.1016/j.enconman.2016.02.075.

References

[1] Ogunkoya D, Fang T. Engine performance, combustion, and emissions study of biomass to liquid fuel in a compression–ignition engine. Energy Convers Manage 2015;95:342–51.
[2] Hunpinyo P, Cheali P, Narataruksa P, Tungkamani S, Chollacoop N. Alternative route of process modification for biofuel production by embedding the Fischer–Tropsch plant in existing stand-alone power plant (10 mw) based on biomass gasification – Part I: A conceptual modeling and simulation approach (a case study in thailand). Energy Convers Manage 2014;88:1179–92.
[3] Rimkus A, Žaglinskis J, Rapalis P, Skačkauskas P. Research on the combustion, energy and emission parameters of diesel fuel and a biomass-to-liquid (btl) fuel blend in a compression–ignition engine. Energy Convers Manage 2015;106:1109–17.
[4] Sarker S, Nielsen HK. Assessing the gasification potential of five woodchips species by employing a lab-scale fixed-bed downdraft reactor. Energy Convers Manage 2015;103:801–13.
[5] Demirbas A. Competitive liquid biofuels from biomass. Appl Energy 2011;88(1):17–28.
[6] Dry ME. The Fischer–Tropsch process-commercial aspects. Catal Today 1990;6(3):183–206.
[7] Leckel D. Diesel production from Fischer–Tropsch: the past, the present, and new concepts. Energy Fuels 2009;23(5):2342–58.
[8] Bezemer GL, Bitter JH, Kuipers HP, Oosterbeek H, Holewijn JE, Xu X, et al. Cobalt particle size effects in the Fischer–Tropsch reaction studied with carbon nanofiber supported catalysts. J Am Chem Soc 2006;128(12):3956–64.
[9] Martinez A, Lopez C, Marquez F, Diaz I. Fischer–Tropsch synthesis of hydrocarbons over mesoporous Co/SBA-15 catalysts: the influence of metal loading, cobalt precursor, and promoters. J Catal 2003;220(2):486–99.
[10] Van de Loosdrecht J, Van der Kraan A, Van Dillen A, Geus J. Metal-support interaction: titania-supported and silica-supported nickel catalysts. J Catal 1997;170(2):217–26.
[11] Jacobs G, Ji Y, Davis BH, Cronauer D, Kropf AJ, Marshall CL. Fischer–Tropsch synthesis: temperature programmed EXAFS/XANES investigation of the influence of support type, cobalt loading, and noble metal promoter addition to the reduction behavior of cobalt oxide particles. Appl Catal A: Gen 2007;333(2):177–91.
[12] Tauster S, Fung S, Baker R, Horsley J. Strong interactions in supported-metal catalysts. Science 1981;211(4487):1121–5.
[13] Storsæter S, Tøtdal B, Walmsley JC, Tanem BS, Holmen A. Characterization of alumina-, silica-, and titania-supported cobalt Fischer–Tropsch catalysts. J Catal 2005;236(1):139–52.
[14] Chu W, Chernavskii PA, Gengembre L, Pankina GA, Fongarland P, Khodakov AY. Cobalt species in promoted cobalt alumina-supported Fischer–Tropsch catalysts. J Catal 2007;252(2):215–30.
[15] Hilmen A, Schanke D, Hanssen K, Holmen A. Study of the effect of water on alumina supported cobalt Fischer–Tropsch catalysts. Appl Catal A: Gen 1999;186(1):169–88.
[16] Jean-Marie A, Griboval-Constant A, Khodakov AY, Diehl F. Cobalt supported on alumina and silica-doped alumina: catalyst structure and catalytic performance in Fischer–Tropsch synthesis. C R Chim 2009;12(6):660–7.
[17] Daniell W, Schubert U, Glöckler R, Meyer A, Noweck K, Knözinger H. Enhanced surface acidity in mixed alumina–silicas: a low-temperature FTIR study. Appl Catal A: Gen 2000;196(2):247–60.
[18] Bessell S. Support effects in cobalt-based Fischer–Tropsch catalysis. Appl Catal A: Gen 1993;96(2):253–68.
[19] Russo N, Mescia D, Fino D, Saracco G, Specchia V. N_2O decomposition over perovskite catalysts. Ind Eng Chem Res 2007;46(12):4226–31.
[20] Hegde M, Madras G, Patil K. Noble metal ionic catalysts. Account Chem Res 2009;42(6):704–12.
[21] Aruna ST, Mukasyan AS. Combustion synthesis and nanomaterials. Curr Opin Solid State Mater Sci 2008;12(3):44–50.
[22] Mukasyan AS, Epstein P, Dinka P. Solution combustion synthesis of nanomaterials. Proc Combust Inst 2007;31(2):1789–95.
[23] Toniolo J, Takimi A, Bergmann C. Nanostructured cobalt oxides (Co_3O_4 and CoO) and metallic Co powders synthesized by the solution combustion method. Mater Res Bull 2010;45(6):672–6.
[24] Prakash A, Khadar A, Patil K, Hegde M. Hexamethylenetetramine: a new fuel for solution combustion synthesis of complex metal oxides. J Mater Synth Process 2002;10(3):135–41.
[25] Patil KC, Aruna S, Mimani T. Combustion synthesis: an update. Curr Opin Solid State Mater Sci 2002;6(6):507–12.
[26] Zavyalova U, Scholz P, Ondruschka B. Influence of cobalt precursor and fuels on the performance of combustion synthesized Co_3O_4/γ-Al_2O_3 catalysts for total oxidation of methane. Appl Catal A: Gen 2007;323:226–33.
[27] Civera A, Pavese M, Saracco G, Specchia V. Combustion synthesis of perovskite-type catalysts for natural gas combustion. Catal Today 2003;83(1):199–211.
[28] Guo X, Mao D, Lu G, Wang S, Wu G. Glycine–nitrate combustion synthesis of CuO–ZnO–ZrO_2 catalysts for methanol synthesis from Co_2 hydrogenation. J Catal 2010;271(2):178–85.
[29] Papavasiliou J, Avgouropoulos G, Ioannides T. In situ combustion synthesis of structured Cu–Ce–O and Cu–Mn–O catalysts for the production and purification of hydrogen. Appl Catal B: Environ 2006;66(3):168–74.
[30] Jess A, Kern C. Influence of particle size and single-tube diameter on thermal behavior of Fischer–Tropsch reactors. Chem Eng Technol 2012;35:379–86.
[31] Shi L, Jin Y, Xing C, Zeng C, Kawabata T, Imai K, et al. Studies on surface impregnation combustion method to prepare supported Co/SiO_2 catalysts and its application for Fischer–Tropsch synthesis. Appl Catal A: Gen 2012;435:217–24.
[32] Shi L, Tao K, Kawabata T, Shimamura T, Zhang XJ, Tsubaki N. Surface impregnation combustion method to prepare nanostructured metallic catalysts without further reduction: as-burnt Co/SiO_2 catalysts for Fischer–Tropsch synthesis. ACS Catal 2011;1(10):1225–33.
[33] LeViness S, Deshmukh SR, Richard LA, Robota HJ. Velocys Fischer–Tropsch synthesis technology-new advances on state-of-the-art. Top Catal 2014;57(6-9):518–25.
[34] Turns SR. An introduction to combustion, vol. 287. New York: McGraw-hill; 1996.
[35] Sewell G, Van Steen E, O'Connor C. Use of TPR/TPO for characterization of supported cobalt catalysts. Catal Lett 1996;37(3–4):255–60.
[36] Medina C, García R, Reyes P, Fierro J, Escalona N. Fischer–Tropsch synthesis from a simulated biosyngas feed over Co(x)/SiO_2 catalysts: effect of co-loading. Appl Catal A: Gen 2010;373(1):71–5.
[37] Trépanier M, Tavasoli A, Dalai AK, Abatzoglou N. Co, Ru and K loadings effects on the activity and selectivity of carbon nanotubes supported cobalt catalyst in Fischer–Tropsch synthesis. Appl Catal A: Gen 2009;353(2):193–202.
[38] Lira E, López CM, Oropeza F, Bartolini M, Alvarez J, Goldwasser M, et al. HMS mesoporous silica as cobalt support for the Fischer–Tropsch synthesis: pretreatment, cobalt loading and particle size effects. J Mol Catal A: Chem 2008;281(1):146–53.
[39] Arnoldy P, Moulijn JA. Temperature-programmed reduction of $CoOAl_2O_3$ catalysts. J Catal 1985;93(1):38–54.
[40] Schanke D, Vada S, Blekkan E, Hilmen A, Hoff A, Holmen A. Study of Pt-promoted cobalt CO hydrogenation catalysts. J Catal 1995;156(1):85–95.
[41] Jabłoński JM, Wołcyrz M, Krajczyk L. On cobalt silicate formation during high-temperature calcination of impregnated cobalt/silica catalysts. J Catal 1998;173(2):530–4.
[42] Patil K, Hegde M, Rattan T, Aruna S. Chemistry of nanocrystalline oxide materials-combustion synthesis, properties and applications. World Scientific; 2008.
[43] O'NEILL H. Temperature dependence of the cation distribution in $CoAl_2O_4$ spinel. Eur J Mineral 1994;6(5):603–9.
[44] Gutiérrez G, Taga A, Johansson B. Theoretical structure determination of γ-Al_2O_3. Phys Rev B 2001;65(1):012101.
[45] Hull AW. X-ray crystal analysis of thirteen common metals. Phys Rev 1921;17(5):571.
[46] Gubicza J, Nauyoks S, Balogh L, Lábár J, Zerda T, Ungár T. Influence of sintering temperature and pressure on crystallite size and lattice defect structure in nanocrystalline SiC. J Mater Res 2007;22(05):1314–21.
[47] Carter J, Cusumano J, Sinfelt J. Catalysis over supported metals. V. The effect of crystallite size on the catalytic activity of nickel. J Phys Chem 1966;70(7):2257–63.

[48] Naumkin AV, Kraut-Vass A, Powell CJ. NIST X-ray photoelectron spectroscopy database. Measurement Services Division of the National Institute of Standards and Technology (NIST) Technology Services; 2008.
[49] Carson G, Nassir M, Langell M. Epitaxial growth of Co_3O_4 on CoO (100). J Vac Sci Technol A 1996;14(3):1637–42.
[50] Ji L, Lin J, Zeng H. Metal-support interactions in Co/Al_2O_3 catalysts: a comparative study on reactivity of support. J Phys Chem B 2000;104 (8):1783–90.
[51] Zsoldos Z, Hoffer T, Guczi L. Structure and catalytic activity of alumina–supported platinum–cobalt bimetallic catalysts. 1. Characterization by X-ray photoelectron spectroscopy. J Phys Chem 1991;95(2):798–801.
[52] Khodakov AY. Enhancing cobalt dispersion in supported Fischer–Tropsch catalysts via controlled decomposition of cobalt precursors. Braz J Phys 2009;39(1A):171–5.
[53] Gardezi SA, Wolan JT, Joseph B. Effect of catalyst preparation conditions on the performance of eggshell cobalt/SiO_2 catalysts for Fischer–Tropsch synthesis. Appl Catal A: Gen 2012;447:151–63.
[54] Fraenkel D, Gates BC. Shape-selective Fischer–Tropsch synthesis catalyzed by zeolite-entrapped cobalt clusters. J Am Chem Soc 1980;102(7):2478–80.
[55] Lu Y, Zhou P, Han J, Yu F. Fischer–Tropsch synthesis of liquid hydrocarbons over mesoporous SBA-15 supported cobalt catalysts. RSC Adv 2015;5 (73):59792–803.
[56] Bukur DB, Lang X. Highly active and stable iron Fischer–Tropsch catalyst for synthesis gas conversion to liquid fuels. Ind Eng Chem Res 1999;38(9):3270–5.
[57] Ail SS, Dasappa S. Biomass to liquid transportation fuel via Fischer–Tropsch synthesis–technology review and current scenario. Renew Sustain Energy Rev 2016;58:267–86.
[58] Di Z, Yang C, Jiao X, Li J, Wu J, Zhang D. A ZSM-5/MCM-48 based catalyst for methanol to gasoline conversion. Fuel 2013;104:878–81.
[59] Triantafyllidis K, Komvokis V, Papapetrou M, Vasalos I, Lappas A. Microporous and mesoporous aluminosilicates as catalysts for the cracking of Fischer–Tropsch waxes towards the production of "clean" bio-fuels. Stud Surf Sci Catal 2007;170:1344–50.
[60] Kibby CL, Jothimurugesan K, Das TK. Process of synthesis gas conversion to liquid fuels using synthesis gas conversion catalyst and noble metal-promoted acidic zeolite hydrocracking–hydroisomerization catalyst. US Patent App. 12/478204, 2009.